BULLETIN OF THE POLISH ACADEMY OF SCIENCES
TECHNICAL SCIENCES, Vol. 68, No. 2, 2020
DOI: 10.24425/bpasts.2020.131845

Compact nanosecond pulse generator based on IGBT and spark gap cooperation

Y. ACHOUR [1]*, J. STARZYŃSKI [2], and A. ŁASICA [2]

[1] Military University of Technology, ul. gen. Sylwestra Kaliskiego 2, 00-908 Warszawa, Poland
[2] Warsaw University of Technology, ul. Koszykowa 75, 00-662 Warsaw, Poland

Abstract. The present paper describes a new architecture of a high-voltage solid-state pulse generator. This generator combines the two types of energy storage systems: inductive and capacitive, and consequently operates two types of switches: opening and closing. For the opening switch, an isolated gate bipolar transistor (IGBT) was chosen due to its interesting characteristics in terms of controllability and robustness. For the closing switch, two solutions were tested: spark-gap (SG) for a powerful low-cost solution and avalanche mode bipolar junction transistor (BJT) for a fully semiconductor structure. The new architecture has several advantages: simple structure and driving system, high and stable controllable repetition rate that can reach 1 kHz, short rising time of a few nanoseconds, high gain and efficiency, and low cost. The paper starts with the mathematical analysis of the generator operation followed by numerical simulation of the device. Finally add a comma the results were confirmed by the experimental test with a prototype generator. Additionally, a comparative study was carried out for the classical SG versus the avalanche mode BJT working as a closing switch.

Key words: pulsed power, nanosecond generator, Isolated Gate Bipolar Transistor (IGBT), spark gap, avalanche mode Bipolar Junction Transistor.

1. Introduction

Since their first appearance, high-voltage pulse generators (HVPG) have undergone many improvements. These improvements were related especially to switching devices, starting with spark gaps (SG) in vacuum and gas-filled tubes and extending to semiconductor switches. All these developments were carried out to meet needs emerging from the applications of HVPG. These applications are still increasing. They started with radar and magnetron development during the Second World War, advanced to nuclear weapon programs in the Cold War era, and presently span unlimited number of usages. A large part of the older applications was collated by Früngel in his four-volume book [1], but new possibilities are still being invented [2].

The general architecture of a high voltage pulse generator is shown in Fig. 1. It contains four main components: the first one is a primary power supply that can be any source of electrical energy: typically a power network or a pack of batteries. The second part is the storage device that can be either capacitive or inductive. It accumulates energy over a longer period and releases it instantaneously to create a short powerful pulse. The third part is the switching system. It plays a very important role because the final pulse shape and characteristics of the whole system depend strongly on the used switches. The principal role of the switch is to control the energy flow within the generator: it connects the storage device to the supply in the first phase, and, it rapidly switches the storage to the load. The last component of the system is the load that depends on the target application.

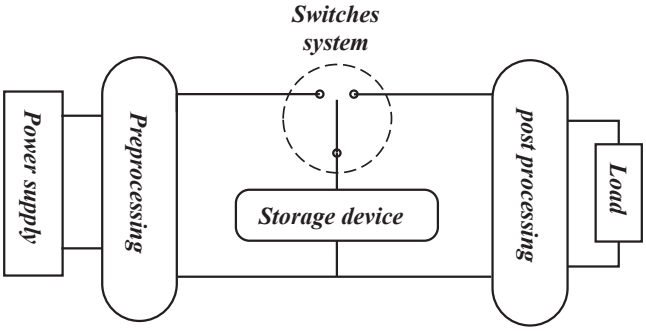

Fig. 1. General architecture of a pulse generator

In reality, many other supplementary parts are necessary for the optimal functioning of the generator. For example a power conditioning, such as a flyback transformer [3], a rectifier or Cockroft–Walton multiplier, may help the power supply to charge the storage device more effectively. For some applications the shape of generated pulses must be further improved by a pulser or a pulse forming network [4, 5]. In most cases, it is inevitable to match the impedance of the generator to that of the load for maximal power transfer. A pulse transformer or a transmission line or a combination of transmission lines (called a Lewis transformer [6]) can be used for this purpose.

Switches in the pulsed power field are generally classified into two categories: closing and opening switches. The first

*e-mail: yahiaaachour@gmail.com

Manuscript submitted 2019-08-14, revised 2019-11-17, initially accepted for publication 2020-01-18, published in April 2020

Table 1
A comparison of properties of different switches

Type	Reference	Voltage (kV)	Current (A)	Rise time (ns)	Controllability	Price ($)
SG	3 mm in air	10	any	5	closing auto	even 1$
IGBT	IXGF30N400	4	30	55	full	55
MOSFET	IXTF1N250	2.5	1	25	full	42.5
SiC-MOSFET	SCT2750NYTB	1.7	5.9	24	full	6
BJT	FMMT417TD	0.32	60	1	closing	11

category is the most popular, and it contains several types of switches such as SG, pseudo spark gaps, and different sorts of gas-filled tubes like thyratrons and ignitrons and other lamps. Many studies described this category. A good overview of gas discharge closing switches can be found in [7]. In addition to that, several semiconductor devices such as thyristors [8, 9], metal-oxide semiconductor field-effect transistors (MOSFET) [10, 11], IGBTs [12, 13] are often used as closing switches in pulsed technology. Typically, this category of switches is combined with capacitive storage. The most popular architecture based on this type is the well-known Marx generator.

The second category (opening switches) is more compatible with inductive storage. It also includes several different types such as fuse opening, explosive-driven switches [14] and, of course, semiconductor switches. A good review of opening switches can be found in [15].

In this work, we present a new generation of low-cost pulse generator designed to be small, portable, and easy to control. It can deliver short and fast pulses of high voltage and low power. Possible applications include biomedical treatments [16] and purification. Some industrial applications include pollution control, testing surge protection devices [17], and the ignition systems in plasma cutting and welding machines, or in electromagnetic pulse (EMP) generation [18, 19].

For such applications, the traditional Marx generator with SG is not convenient due to several reasons. First, its voltage gain is proportional to the number of stages, which implies that the generator size is proportional to the output voltage. Second, the repetition rate is not controllable because it depends on the oscillation of the RC circuit and it is also limited by the recovery time of the SG. Additionally the traditional Marx generator needs a high voltage supply, which makes the system heavier, more expensive, and less efficient. All these limitations favour the development of other alternative solutions such as generators based on semiconductor switches.

This type of designs has received tremendous interest in recent decades due to their numerous advantages (especially those using MOSFETs or IGBTs) [20–24]: they can provide quasi-square pulses with controllable repetition rate and pulse-width and have much more compact structure.

Many of the modern solutions inherit Marx generator architecture and substitute SG by semiconductor switches [25, 26], while other solutions are based on boost converter topology [27, 28] or some other structures [29, 30]. However, almost all of these generators cannot provide fast rising pulses. This weakness is caused by the dynamics of the semiconductor switches, which can reach 20 ns in the best cases. Fast semiconductor switches with nanosecond rise time, such as semiconductor opening switches (SOS) [31] and drift step recovery diodes (DSRD) [32–34], were proposed, but they are not available in the market. Another interesting alternative is the avalanche mode bipolar junction transistor (BJT). Studies covering these devices started in the early fifties [35] and continue to date [36]. Avalanche BJT is really very fast (it's rise time can reach 1 ns), and the jitter is very low. However, the power range for these devices is limited, especially the voltage that cannot exceed some hundreds of volts. The series connection to raise the voltage capabilities is possible, but it raises the cost of the generator. The quest for a solution to this problem guided us to a new design.

The idea of the design presented in this paper is to combine the two types of switches to obtain better performance by exploiting their advantages. To achieve the goal, we have profoundly studied each of them to determine the pros and cons. The main properties of different types of switches are illustrated in Table 1. Based on this comparison, we attempted to create the best possible fusion: an SG was chosen as the main switch due to its fast switching, high power range, simple structure, and low cost. Its drawbacks, such as complex triggering and low repetition rate, were overcome by combining it with an IGBT working as an opening switch. IGBTs are very successful in power electronics and motor driving due to their power range and full controllability in closing and opening. They have also small size, simple driving system, and fast switching capabilities. This makes them convenient to use with micro-controllers and digital processors.

It is worth mentioning that, in the pulsed power field, the IGBTs are usually used as closing switches, as in [12, 13, 25–27, 37]. Its application as an opening switch is rare. One of the purposes of the presented paper is to show the advantages of such a solution.

In the next sections, the general architecture of the proposed generator is presented and analyzed. Results of the theoretical study are supported by computer simulation and some laboratory tests.

2. Functioning principle

The proposed generator consists of an inductor, an IGBT, a diode, a capacitor, an SG, or an avalanche mode BJT as discussed later, and a load as shown in Fig. 2.

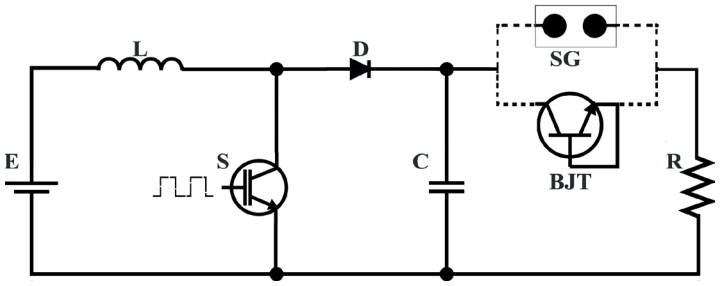

Fig. 2. Architecture of the new high voltage pulse generator. Two versions: first with a spark gap and second with an avalanche BJT are shown

The operational cycle can be divided into four phases. In the first phase, the energy flows from the input supply to the inductor through the closed IGBT. The second phase starts when the IGBT opens and the current changes its path, thereby charging the capacitor. The serial connection of the inductor and the capacitor creates a high gain of charging voltage. The third phase starts when the voltage across the capacitor exceeds the breakdown value of the SG and a very short pulse occurs across the load. After the discharge of the capacitor and the end of the spark, the system enters the fourth phase, waiting for the next closing of the IGBT.

The functioning principle of this generator was briefly explained in [38]. In the following paragraphs, we will explain every step in detail in order to deduce the general equations that describe the model.

2.1. The first phase: inductive storage. Initially, the capacitor is fully discharged, and the IGBT and the diode are off: therefore no current flows in the circuit. When the IGBT is turned on by the control unit, the current starts to flow from the DC supply through the inductor and through the IGBT back to the source. Consequently, the inductor starts storing energy. The current rises linearly according to equation (1) as shown in Fig. 3 (phase 1).

$$I_L(t) = \frac{E}{L} \cdot t \tag{1}$$

The IGBT is controlled to be closed after an interval T_{on} called the activation time. During the activation time the inductor current raises, reaching its final value I_0 given by (2). This phase ends by switching off the IGBT.

$$I_0 = I_L(T_{on}) = \frac{E}{L} \cdot T_{on} \tag{2}$$

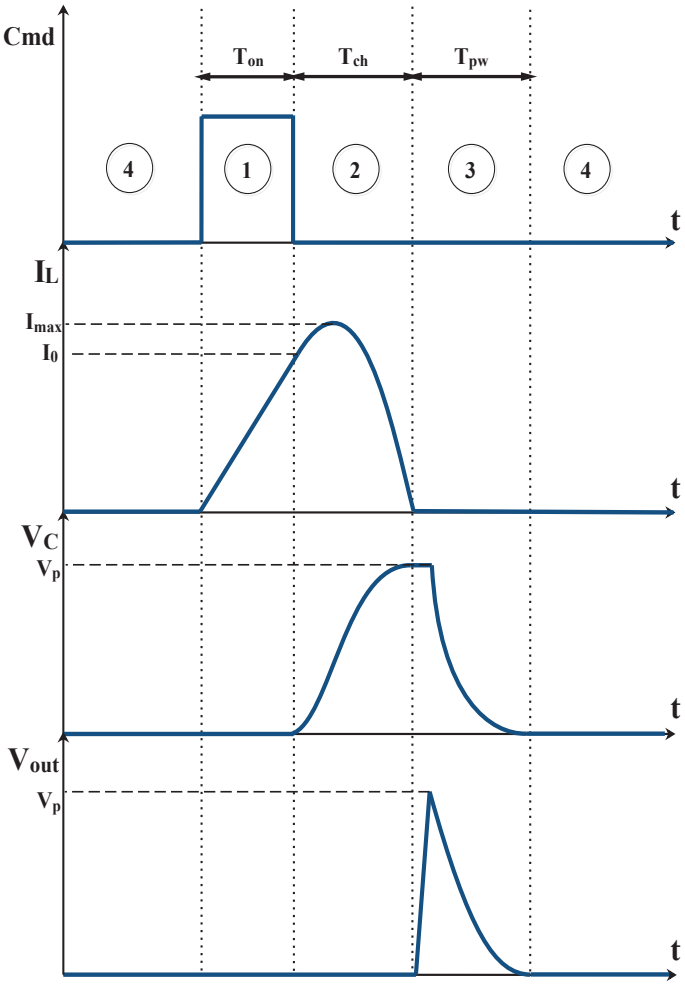

Fig. 3. Main system signals from top to bottom: IGBT triggering signal; inductor's current I_L; capacitor's voltage V_C; output voltage V_{out}. The phases of operation are indicated by numbers in circles

2.2. The second phase: charging of the capacitor. After switching off the IGBT, the inductor current is forced to pass through the capacitor, thereby charging it. The equivalent circuit of the generator in this phase can be represented by a voltage source connected in series with an inductor and a capacitor. The voltage across the capacitor can be obtained by solving the differential equation (3).

$$V_C = E - L \cdot \frac{dI_L}{dt} \tag{3}$$

Analysing (3) we can notice that the capacitor is charged in two steps: the first when $E > V_C$, in this step the current still rises, which means that the energy of inductor is still increasing. In other words, the DC supply provides energy for both the inductor and capacitor. The second step starts when the voltage across the capacitor becomes higher than the input voltage ($V_C > E$). Then, the current starts decreasing and both the DC supply and the inductor transfer their energy to the capacitor and finally make it overcharged.

The dynamics of the inductor current is governed by the second order differential equation

$$\frac{d^2 I_L}{dt^2} + \omega^2 \cdot I_L = 0 \tag{4}$$

with the initial condition $L(0) = I_0$ given by (0) at the end of the first phase. The natural frequency of the circuit ω is determined by the capacitance and inductance:

$$\omega = \frac{1}{\sqrt{C \cdot L}}. \tag{5}$$

Solving equation (4), we obtain the general current expression given as:

$$I_L(t) = I_{max} \cdot \sin(\omega \cdot t + \phi) \tag{6}$$

where $I_{max} = \sqrt{I_0^2 + \frac{E^2}{L^2 \cdot \omega^2}}$ is the maximal current and ϕ is the phase shift given by $\phi = \operatorname{atan}\left(\frac{I_0 \cdot L \cdot \omega}{E}\right) = \operatorname{atan}(\omega \cdot T_{on})$. Integrating this solution, we can derive the expression for the maximal capacitor voltage V_p given by

$$V_{ch} = E \cdot \left(1 + \sqrt{1 + \omega^2 \cdot T_{on}^2}\right). \tag{7}$$

For small values of the inductance and capacitance, the product of the natural pulsation times the activation time becomes much higher than 1, so we can approximate the output pulse voltage with the linear equation:

$$V_{ch} \approx E \cdot (1 + \omega \cdot T_{on}). \tag{8}$$

Formulas (7) and (8) show that the output pulse voltage V_{ch} is a function of activation time T_{on} and also of the natural frequency of the LC circuit that reflects the resonance phenomena between the inductor and the capacitor. This allows to amplify the input voltage and charge the capacitor with a substantially higher voltage than the supply.

The ratio between the output pulse magnitude and the input (charging voltage) is always higher than 2 and almost linearly dependent on T_{on}. It can be very high, in theory infinite, according to (7), but in reality, it is limited because the charging current is limited by the inductors' resistance (neglected in this model for simplification reasons).

The second phase ends when the inductor current crosses zero, which corresponds to switching the diode off. From (6), we can deduce the length of this phase. The charging time T_{ch} is given as

$$T_{ch} = \frac{\pi - \phi}{\omega}. \tag{9}$$

2.3. The third phase: discharging of the capacitor. When the capacitor voltage exceeds the breakdown voltage of the SG, the gas between the electrodes is ionized, and the current commences to flow from the capacitor through the load. The rise time of the output voltage is controlled by the dynamics of the ionization within the SG and the parasitic inductance of the capacitor and the wires (and, eventually, the load).

SG setup. For best performance of the generator, the breakdown voltage (which is the same as the pulse amplitude) denoted V_p should be equal to the maximal charging voltage of the capacitor, i.e., $V_p = V_{ch}$. For a given SG, we can adjust this value by changing the distance between the electrodes or the pressure of the gas. However, one should remember that these factors will influence the dynamics of the switch. We note that if the breakdown voltage is lower than the charging one $V_p < V_{ch}$, then the SG switches on before the capacitor is fully charged. If it is higher $(V_p > V_{ch})$, the breakdown will never occur or will eventually occur after accumulating energy from several charging cycles.

To sustain the ionisation between the electrodes of the SG, the current should be higher than a specific value called the maintenance current [39]. After the discharge, the capacitor cannot provide the required current to maintain the ionisation and the SG switches off. Depending on the load, the discharge of the capacitor could be faster or slower. The time needed for that operation is called the pulse width and denoted T_{pw}. For resistive load, the discharging time can be estimated as the circuit time constant multiplied by five.

$$T_{pw} = 5 \cdot R \cdot C \tag{10}$$

BJT as an alternative to SG. Avalanche BJTs are based on a phenomenon called current mode second breakdown, which can be destructive, but for a short time, BJT may be used as a fast, low jitter, high-voltage switch [40]. In this mode, the voltage across the BJT is switched from its maximal value to a very small one in a very short time and then current rises dramatically, hence the name "Current mode second breakdown". The BJT can be forced to switch by triggering its base, but in the present design, it is used in the auto-firing mode. In this case, it behaves exactly like an SG.

When using avalanche BJT instead of SG (shown as an option in Fig. 2), the breakdown voltage is a characteristic of the device that cannot be adjusted. On average, the breakdown voltage of a single BJT is a few hundred of volts. A series connection of several BJTs is always enables to reach a higher voltage.

2.4. The fourth phase. By the end of the spark between the electrodes (or switching the BJT off), the capacitor is fully discharged. The IGBT and the diode remain opened. The system waits for the next triggering signal from the control unit to repeat the cycle.

3. Discussion

Analysis of the generator's operation, presented in the previous chapter, shows that that the cooperation of both switches allows

for using their strengths. The IGBT, which has a long switching time and cannot handle high current, is not adequate as the main switch for the capacitor discharge. However, it is fully controllable with a simple driving circuit, which makes it perfect for interface with the control unit. On the other hand, the SG is hardly controllable, but its power capabilities and fast operation makes it perfect for discharging the capacitor. Summing up, the generator operation combines two pulses: the first is a slow current pulse controlled by the IGBT to charge the capacitor, the second is a fast voltage pulse controlled by the SG. This can be observed in Fig. 3 (compare the slope of the current in the first phase and the slope of the voltage at the beginning of the third phase).

We note that the IGBT is working in the soft switching mode. It switches on in the zero current switching mode (ZCS) and switches off in the zero voltage switching mode (ZVS) [41]. That implies that the IGBT switches only when its current or voltage is zero. Contrary to the hard switching mode, the soft one has several advantages such as minimizing the switching losses and extending the IGBT's lifetime.

To predict the theoretical maximal repetition rate of the generator we can calculate the time needed for phases 1–3 (see Fig. 3):

$$RR_{max} = \frac{1}{T_{on} + T_{ch} + T_{pw}}. \tag{11}$$

It is very important to understand that in practice, there are two main parameters that limit the repetition rate. The first one RR_{max}, which is already discussed, is determined by the design of the system. However, the practical repetition rate is also limited by the dynamics of the SG. In general, the repetition rate of SG is very limited, especially at ambient pressure. It is one of the major limitations of SG.

Yet another point is that the used SG is not externally triggered. The breakdown occurs naturally when the voltage between the electrodes becomes higher than the limit given by Paschen's law. This may cause a relatively high jitter, which makes this design unsuitable for some applications that need high time precision. We will return to this issue later in this article.

We also note that the output pulse is highly exponential. Double exponential pulse pulses have some applications, for instance, testing equipment for electromagnetic compatibility as in MIL-STD-461 standard test RS105. However, the new tendency is to use rectangular or bipolar pulses in such tests because of their high harmonic contents. The present generator in its current state can not create rectangular pulses. However, by connecting a Blumlein line at the output, we could generate perfect rectangular pulses with pulse width as short as 10 ns.

Finally, the limited lifetime of SG cannot be ignored. In general, the SG lifetime is measured by the maximal accumulated quantity of charge that the SG can pass. If the quantity of charge per shot is high, the maximal number of shots will be limited. However, the proposed design is dedicated for low power application; hence, the lifetime in terms of the number of shots should not be an issue.

4. Simulation

To assess the previous mathematical model, a first numerical simulation, shown in Fig. 4, was performed using ANSYS Simplorer [43].

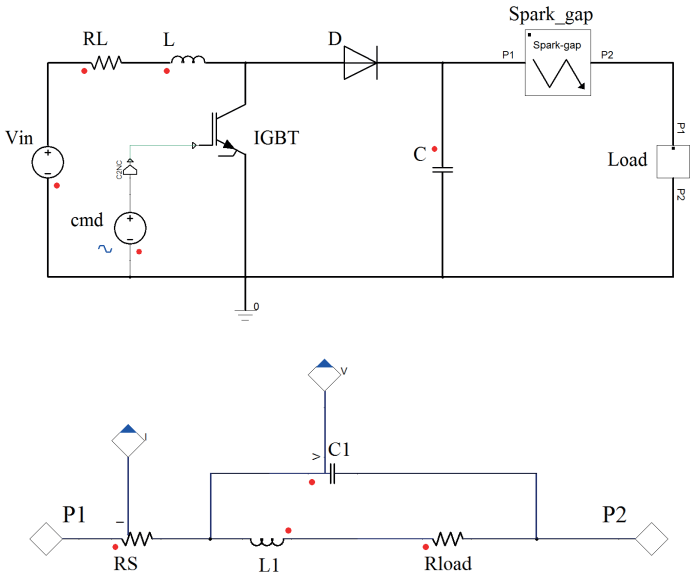

Fig. 4. Model of the generator and the load in ANSYS Simplorer

The simulation used a simple linear coil model: an inductance with a resistor in series to model the resistance of the winding. The spark gap model was constructed according to [44] with the threshold voltage set to 1.2 kV. The other parameters were taken as follows:

- Coil: L = 1 mH with a resistance RL of 50 mΩ;
- Capacitor: C = 4 nF;
- Input voltage: 25 V;
- Repetition rate: 100 pps;
- Load resistance: 100 Ohm.

For the considered range of frequency, modelling the load as a single resistor is not accurate; hence, we have used a serial connection of a resistor with 10 uH inductance, and parallel with 20 pF capacitance as shown in Fig. 4. The connectors were modelled as a small resistance of 1 mΩ.

The obtained results are presented in Fig. 5. The current and voltage waveforms are very close to those predicted by the theoretical simplified model, with some differences caused by the simplifications of the analytical model. The most important one is that the capacitor voltage is never zero because when the IGBT is open, a small current flows from the supply to the capacitor and charge it. However, in the present study, we are interested in high voltage gain, which means that the input voltage can be neglected compared to the output one.

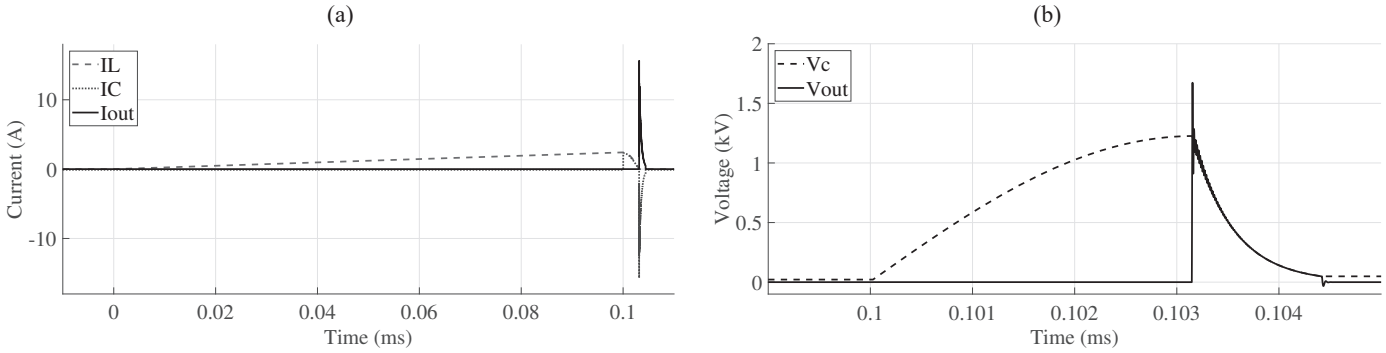

Fig. 5. Simulated waveforms (activation time: 100 µs): a) Current through: the inductor (dashes), the capacitor (points), the load (continuous); b) Voltage across: the capacitor (dashes), Output voltage (continuous)

4.1. Realistic model of the coil. To ascertain the influence of the inductor core saturation on the functioning of the generator, a second simulation was performed. The simulation used a high fidelity finite element model of the inductor that was elaborated using ANSYS Maxwell 3D. This model was incorporated into the global Simplorer model of the generator to observe the influence of this saturation and, the losses inside the magnetic material on voltage gain, and the power efficiency of the generator. The used inductor geometry is shown in Fig. 6. The magnetic core is made of Ferrite 3F3. The magnetic characteristics of this material are given in [42]. In Fig. 7, the obtained results are compared to those of the first simulation.

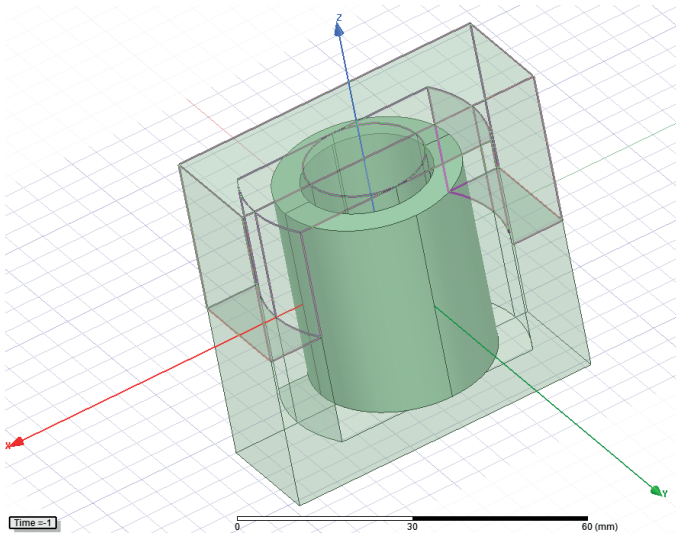

Fig. 6. FE model of the inductor in ANSYS Maxwell 3D

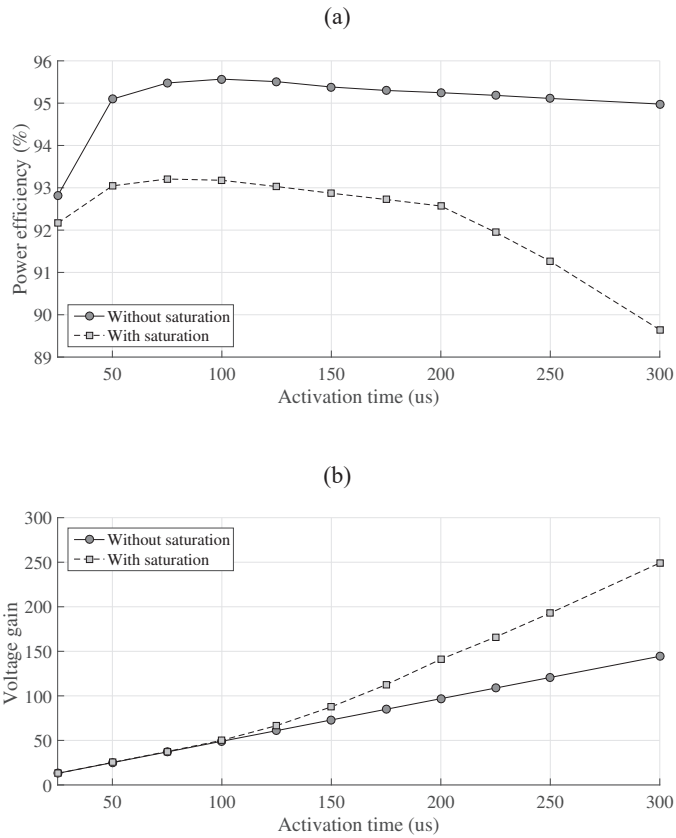

Fig. 7. Simulated influence of the core saturation on the power efficiency and voltage gain: a) Power efficiency as a function of activation time; b) Voltage gain as a function of activation time

Study of the effect of the inductor saturation on the behaviour of the generator is important for many reasons: the first is that the core size should be possibly reduced because it represents a large part of the generator weight. The minimization of the inductor size will inevitably introduce the saturation effect. The second reason is the influence of the core losses on the generator power efficiency. It is obvious that maximization of the power efficiency will increase the autonomy of the device.

Figure 7a shows the power efficiency of the generator, calculated for both models, as a function of the activation time T_{on}. It is clear that the second model shows lower efficiency, taking into account more losses than the first one. This difference is more evident for $T_{on} > 200$ µs when the saturation occurs.

Both models predict maximal efficiency for $T_{on} = 100$ µs. This can be explained by the fact that for maximum power transfer between the LC circuit and the supply, an impedance matching condition should be met. In other words, the inductor's resistance plus the DC supply impedance should be equal to the effective input impedance of the generator which is a function of the activation time and the LC parameters. In the presented case, it corresponds to $T_{on} = 100$ µs.

By analyzing the voltage gain dependency shown in Fig. 7b, we note that for the linear model, the voltage is a linear function of T_{on} as predicted by (8). However, when the saturation occurs, we observe a considerably higher gain of the voltage. This difference can be explained by reviewing (5) and (8). According to these formulas, the voltage gain is inversely proportional to the square root of the inductance: when the magnetic core becomes saturated, the inductance decreases; this in turns gives a higher gain.

5. Experimental results

To validate the proposed design, a small prototype generator was built and tested in the High Voltage Laboratory of the Faculty of Electrical Engineering at Warsaw University of Technology. Figure 8 shows a photo of the built generator and the measurement test bench. The generator is powered by two 12 V batteries connected in series and used as a DC supply. It consists of a 12 kV/30 A IGBT, an optically triggered switch, a 4 nF high voltage capacitor, a 1 mH inductor, and a spark gap.

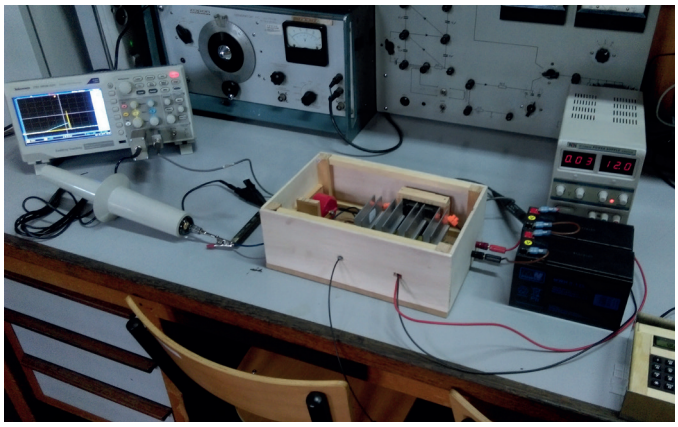

Fig. 8. Photo of the experimental test bench

The choice of the real system's parameters, such as capacitance and inductance, was made to fulfil some constraints: the chosen capacitance depends on the load and the quantity of charge required to obtain the pulse width suitable for the targeted application. The inductance is then calculated according to equations (5–9) to obtain the minimum charging time. However, the IGBT current should not exceed the maximal tolerated value. A high current will, of course, limit the IGBT lifetime.

A typical example of the obtained waveforms is shown in Fig. 9. Two pulses can be distinguished from the figure: the slow current pulse (in green) controlled by the IGBT, and the fast voltage pulse (in blue) controlled by the SG. These results truly validate the synergy of the two switches.

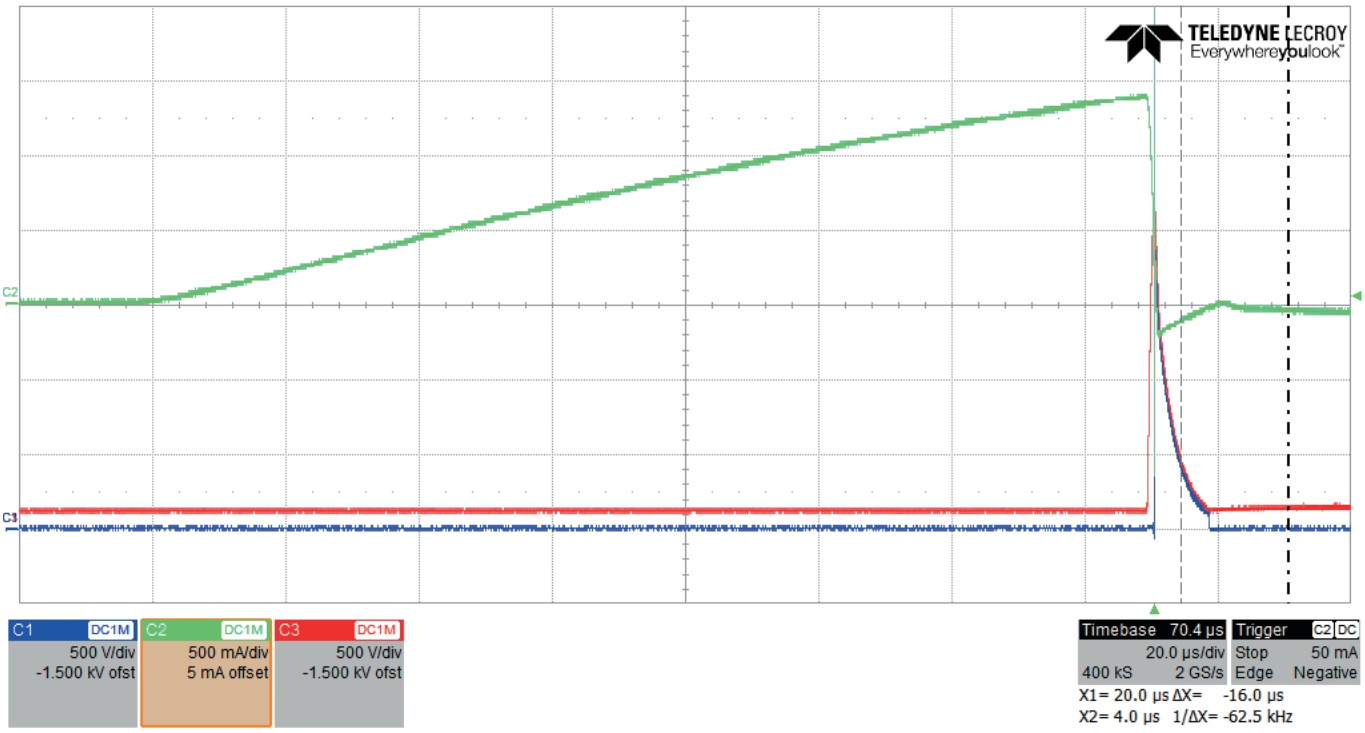

Fig. 9. Experimental waveforms: inductor current (green); output pulse (blue); capacitor's voltage (red)

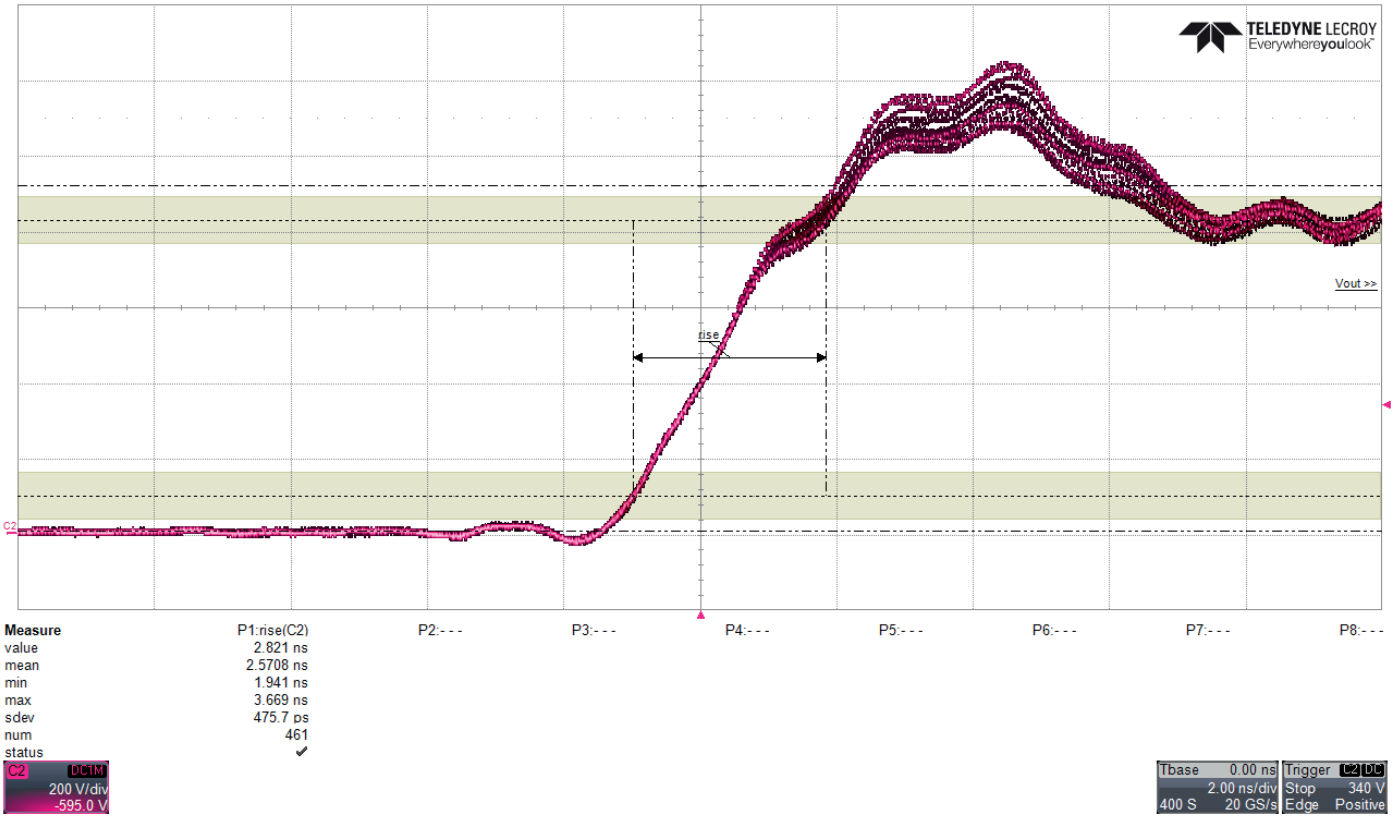

Fig. 10. The rising edge of the output voltage (461 pulses), zoomed to illustrate pulse reproducibility

Figure 9 was recorded using 762 Ω resistance load and 150 µ activation time, which were chosen for better visualization. All the following results were obtained using 100 Ω load and 100 µ activation time, which corresponded to the maximal power efficiency predicted by the simulation.

Figure 10 shows a zoom on the rising edges of the output pulse. The figure shows 461 overlaying pulses. The average value of the rise time was estimated as 2.57 ns by using the oscilloscope. This figure also confirms the reproducibility of the pulses and the sustainability of the generator.

Another important test was carried out to determine the maximal repetition rate allowed by the generator. The generator reached 1000 pps with a very stable repetition rate and without any abnormalities. The results are shown in Fig. 11. The upper inset shows the waveform in the real time scale, while the bottom one is a zoom of the pulses. It is clear that even at this repetition rate, the output pulses are very similar, which is yet another confirmation of the sustainability of the proposed design.

As mentioned before, the use of SG working in auto breakdown mode without any external triggering creates some problems—especially the jitter. To estimate the precision of the proposed generator we studied the jitter time between the IGBT triggering signal and the SG breakdown.

The generator was fired for 2000 times at the repetition rate of 100 pps. The delay between the triggering signal and the real output pulse was measured and recorded. More precisely, the delays between turning off the IGBT and the breakdown of the SG were gathered in files and analyzed statistically. The results are presented in Fig. 12. It shows the histogram of the delays. The delays vary from 3.16 µs to 3.85 µs which implies the maximal jitter of about 700 ns. More statistical parameters were calculated as follows: the mean value of 3.4 µs represents the time needed to charge the capacitor (T_{ch}). The standard deviation of this value was 100 ns.

Finally, the following parameters of the generator were obtained for 100 µs activation time and 100 Ω load:

- Voltage gain: 50;
- Output pulse voltage: 1.2 kV;
- Rise time: 2.57 ns;
- Pulse width: 1 µs;
- Maximal stable repetition rate: 1000 pps.

In the second part of experiments, we replaced the SG with an avalanche BJT switch made by connecting 10 transistors in series. All transistors are identical (FMMT417TD, a product of Diodes Incorporation) with the maximal breakdown voltage of 320 V. The obtained results are presented in Fig. 13, which shows two pulses. The first (the upper inset) was obtained using 100 Ω load. The pulse shape is very similar to the previous configuration, but it has a shorter rise time (around 1 ns) and lower jitter. However, when the load is high (50 kΩ), as shown in the bottom inset of Fig. 13, the BJT cannot stay in the secondary breakdown mode for a long time due to the low current. After 300 ns, it switches to the primary avalanche

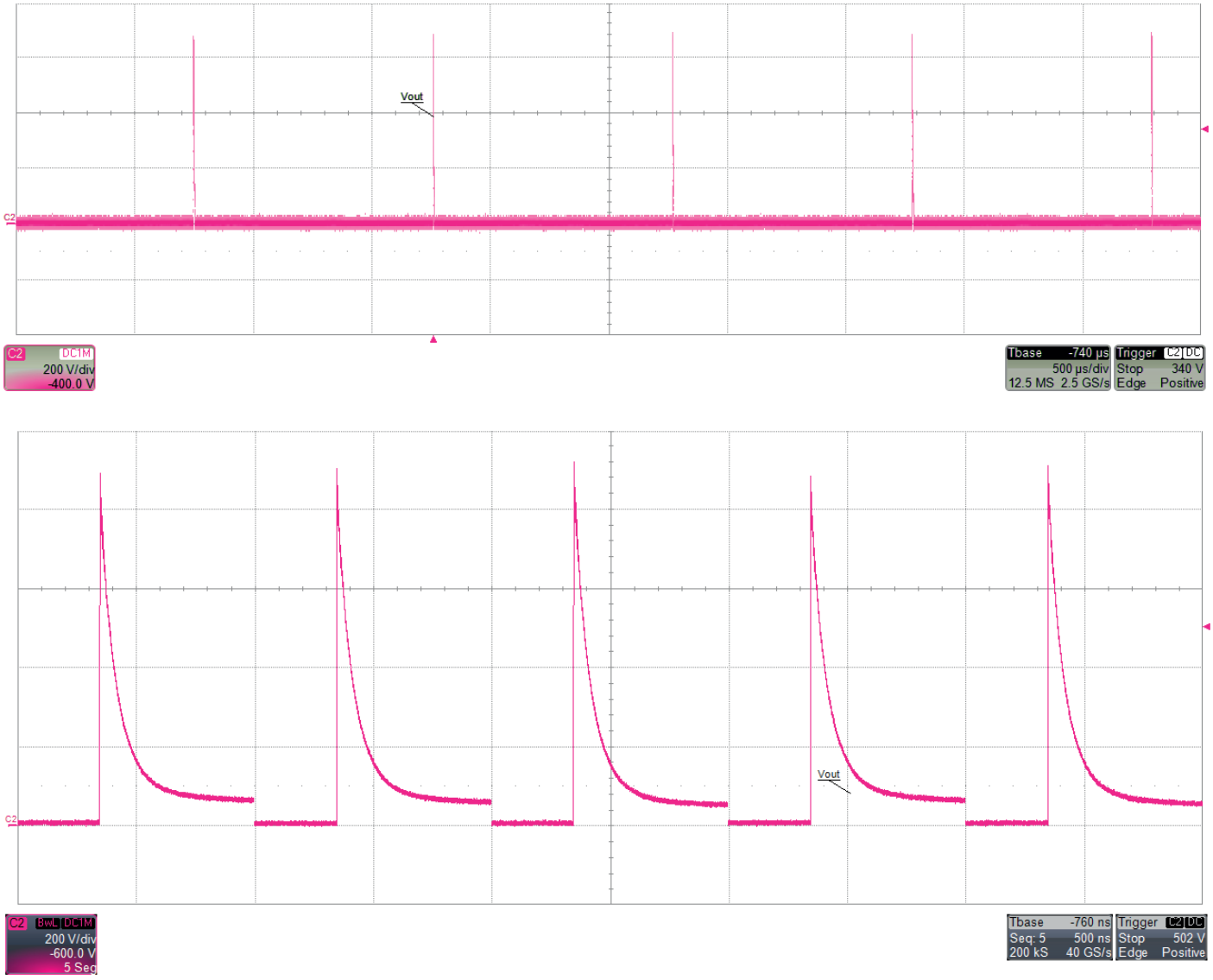

Fig. 11. Sequential test at the repetition rate of 1 kpps

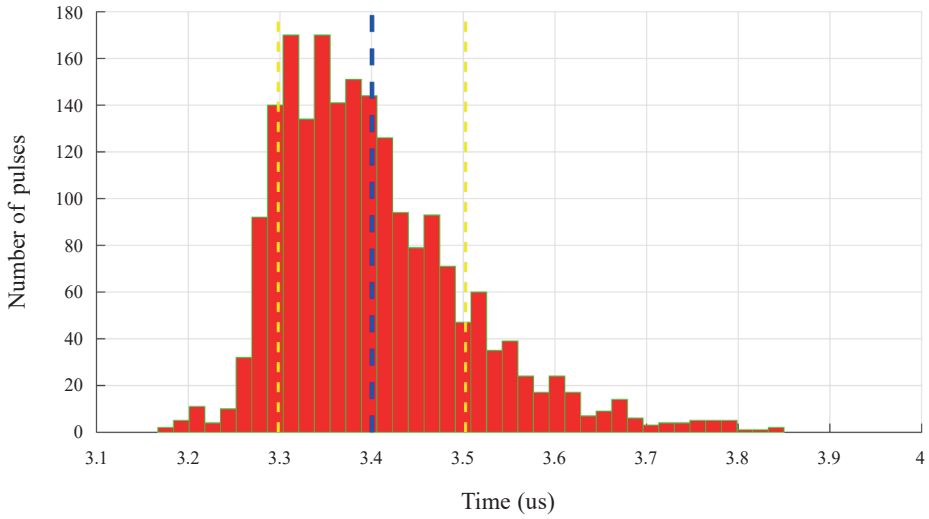

Fig. 12. Delay histogram (jitter estimation test)

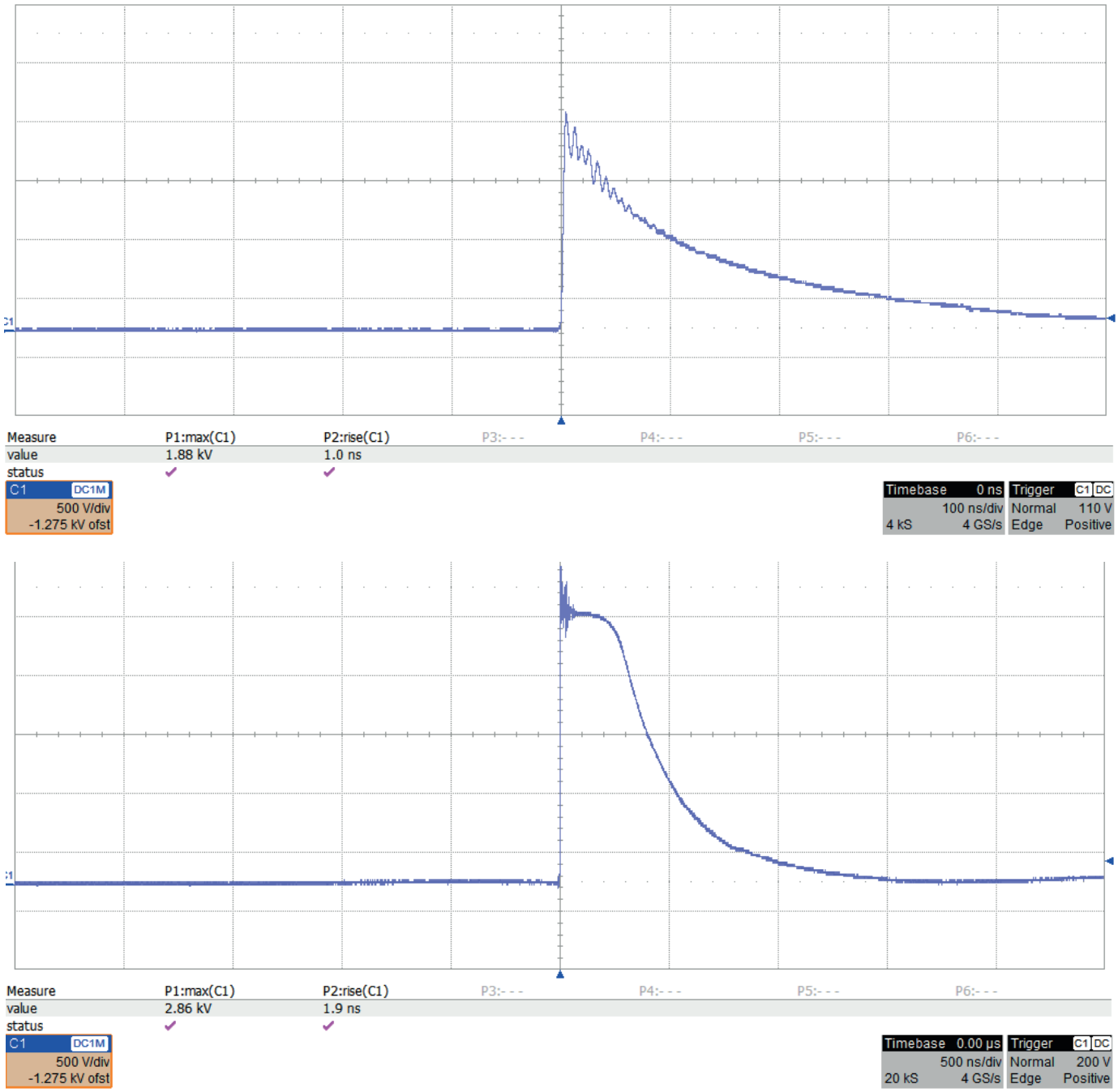

Fig. 13. Generated pulses using avalanche BJT

mode where the voltage across the BJT is not zero, which creates a power dissipation in the transistor. Hence, BJTs are not recommended for applications that require long pulses. Additionally, we can observe a significant difference in pulse magnitude: for 100 Ω load, it reaches 1.88 kV and for 50 kΩ loads – 2.86 kV. The difference is caused by a voltage drop on the BJT switch, which even when on, shows noticeable impedance.

Summarizing, the use of BJT as the main switch instead of an SG has several advantages such as faster switching, lower jitter and high repetition rate. However, it also has some limitations regarding the voltage level, the maximal current that set measures to the load, and a limited pulse width. Additionally, the cost of BJT is significantly higher.

6. Conclusion

A new architecture of a pulse generator was proposed. Fundamentally it uses the synergy of two types of switches: opening

(IGBT) and closing (SG or avalanche mode BJT), and two types of storage systems: inductive and capacitive.

A mathematical description extended by ANSYS Simplorer and Maxwell 3D simulations was used to design the generator. A reduced prototype was then built in the laboratory and tested. All results prove the validity of the proposed design. Based on the experimental results, a comparison was performed between SG- and avalanche BJT-based variants of the device. Additionally, an experimental estimation of the jitter time of the spark gap was performed.

Table 2
Comparison between the two generators

Characteristics	SG	BJT
rise time (ns)	2.57	1
minimum load (Ω)	–	50
jitter	few µs	≤ 1 ns
pulse width limits	no	≤ 500 ns
switch cost ($)	≤ 1	110

Comparing to the other structures reported in the literature, the proposed one has several advantages such as a very compact and simple structure, low voltage supply, fast switching and high repetition rate, high power efficiency and high voltage gain. These features make the generator very convenient for embedded applications.

The basic generator architecture with SG has some limitations such as limited repetition rate, high jitter and the necessity to regularly clean the electrodes. However, for low power application, these limitations are not crucial. For more precise firing with a higher repetition rate, the use of avalanche BJT is recommended at the expense of the higher cost and lower power limits.

Acknowledgements. The ANSYS software used in this work was provided by the partnership agreement of ANSYS Inc., MESco Poland and Warsaw University of Technology.

References

[1] F. Früngel: High speed pulse technology, Academic Press, 1965.
[2] H.A. Ryan, S. Hirakawa, E. Yang, C. Zhou, and S. Xiao, "High-Voltage, Multiphasic, Nanosecond Pulses to Modulate Cellular Responses", *IEEE Transactions on Biomedical Circuits and Systems* 12(2), 338–350 (2018).
[3] Y. Achour and J. Starzyński, "High-frequency displacement current transformer with just one winding", *COMPEL – The international journal for computation and mathematics in electrical and electronic engineering* 38(4), 1141–1153 (2019).
[4] C.R. Rose, "Type-E pulse-forming-network theory and synthesis", *Pulsed Power Conference (PPC)*, (2015).
[5] H. Ghawde and R. Harchandani, "Comparison of pulse forming networks for Marx generator", International Conference on Nascent Technologies in Engineering (ICNTE), (2017).
[6] I.A.D. Lewis, F.H. Wells: Millimicrosecond Pulse Techniques, Second Edition, Pergamon science series electronics and waves, PERGAMON press, (1959).
[7] G. Schaefer, M. Kristiansen, A.H. Guenther: Gas Discharge Closing Switches, Advances in Pulsed Power Technology, Springer US, (2013).
[8] Y. Kozasa, S. Sato, T. Sugai, W. Jiang, A. Tokuchi, M. Akemoto, and H. Nakajima, "Solid-state Marx generator for interna tional linear collider", *IEEE International Power Modulator and High Voltage Conference (IPMHVC)*, 701–704 (2014).
[9] R. Stala, S. Pirog, A. Penczek, A. Kawa, Z. Waradzyn, A. Mondzik, and A. Skała, "A family of high-power multilevel switched capacitor-based resonant DC-DC converters – operational parameters and novel concepts of topologies", *Bull. Pol. Ac.: Tech*. 65(5), 639–651 (2017).
[10] J. Perez, T. Sugai, A. Tokuchi, and W. Jiang, "Marx Generators Based on MOS-Gated Switches With Magnetic Assist for Accelerator Applications", *IEEE Transactions on Plasma Science* 46(6), 2114–2119 (2018).
[11] J. Rąbkowski and T. Płatek, "A study on power losses of the 50 kVA SiC converter including reverse conduction phenomenon", *Bull. Pol. Ac.: Tech*. 64(4), 907–914 (2016).
[12] C. Yao, S. Dong, Y. Zhao, Y. Mi, and C. Li, "A Novel Configuration of Modular Bipolar Pulse Generator Topology Based on Marx Generator With Double Power Charging", *IEEE Transactions on Plasma Science* 44(10), 1872–1878 (2016).
[13] S. Zabihi, Z. Zabihi, and F. Zare, "A solid-state Marx generator with a novel configuration", *19th Iranian Conference on Electrical Engineering (ICEE)*, (2011).
[14] M. Balcerak, R. Pałka, and M. Hołub, "High voltage pulse generation using magnetic pulse compression", *Archives of Electrical Engineering, Polish Academy of Sciences* 62(3), (2013).
[15] A.H. Guenther, T. Martin, M. Kristiansen: Opening Switches, Advances in Pulsed Power Technology, Springer US, (2012).
[16] Y. Achour, J. Starzyński, W. Kasprzycka, and E.A. Trafny, "Compact low-cost high-voltage pulse generator for biological applications", *International Journal of Circuit Theory and Applications* 47(12), 1948–1962 (2019).
[17] M. Szewczyk, "Multi-spark modeling of very fast transient overvoltages for the purposes of developing HV and UHV gasinsulated switchgear and of conducting insulation co-ordination studies", *Bull. Pol. Ac.: Tech*. 65(6), 871–882 (2017).
[18] Y. Achour, J. Starzyński, and A. Josko, "Nanosecond EMP simulator using a new high voltage pulse generator", *Przeglad Elektrotechniczny* 93(10), 33–36 (2017).
[19] Y. Achour, J. Starzyński, A. Josko, and M. Suproniuk, "D-dot, Bdot Data Processing of Fields Generated with Broadband Pulsed Antenna", *Przeglad Elektrotechniczny* 95(11), 109–112 (2019).
[20] M. Hochberg et al., "A Fast Modular Semiconductor-Based Marx Generator for Driving Dynamic Loads", *IEEE Transactions on Plasma Science* 47(1), 627–634 (2019).
[21] M. Hochberg, M. Sack, D. Herzog, A. Weisenburger, and G. Mueller, "Design Validation of a Single Semiconductor-Based Marx-Generator Stage for Fast Step-Wise Arbitrary Output Waveforms", *IEEE Transactions on Plasma Science* 46(10), 3284–3290 (2018).
[22] Z. Li, H. Liu, S. Jiang, and J. Rao, "A novel drive circuit with overcurrent protection for solid state pulse generators", *IEEE Transactions on Dielectrics and Electrical Insulation* 26(2), 361–366 (2019).

[23] Y. Liu, R. Fan, X. Zhang, Z. Tu, and J. Zhang, "Bipolar high voltage pulse generator without H-bridge based on cascade of positive and negative Marx generators,", *IEEE Transactions on Dielectrics and Electrical Insulation* 26(2), 476–483 (2019).

[24] C.Wang, B. Yuan, J. Mao, and W. Shi, "High Repetition Frequency and High Voltage Pulse Generator Research Based on NLTLs", *International Conference on Microwave and Millimeter Wave Technology (ICMMT), Chengdu*, 1–3 (2018).

[25] S. Zabihi, F. Zare, G. Ledwich, A. Ghosh, and H. Akiyama, "A new family of Marx generators based on commutation circuits", *IEEE Transactions on Dielectrics and Electrical Insulation* 18(4), 1181–1188 (2011).

[26] S. Zabihi, Z. Zabihi, and F. Zare, "A Solid-State Marx Generator With a Novel Configuration", *IEEE Transactions on Plasma Science* 39(8), 1721–1728 (2011).

[27] J.W. Baek, M.H. Ryu, D.W. Yoo, and H.G. Kim, "High voltage pulse generator using boost converter array", *IEEE 28th Annual Conference of the Industrial Electronics Society (IECON)*, 395–399 (2002).

[28] M. Taherian, M. Allahbakhshi, E. Farjah, and H. Givic, "A Modular Topology of Marx Generator Using Buck–Boost Converter", *IEEE Transactions on Plasma Science* 47(1), 549–558 (2019).

[29] L. Yu, Z. Jiu, T. Sugai, A. Tokuchi, and W. Jiang, "Pulsed Voltage Adder Topology Based on Inductive Blumlein Lines", *IEEE Transactions on Plasma Science* 46(5), 1816–1820 (2018).

[30] M.R. Kazemi, T. Sugai, A. Tokuchi, and W. Jiang, "Waveform Control of Pulsed-Power Generator Based on Solid-State LTD", *IEEE Transactions on Plasma Science* 45(2), 247–251 (2017).

[31] S.K. Lyubutin, G.A. Mesyats, S.N. Rukin, and B.G. Slovikovskii, "Repetitive nanosecond all-solid-state pulsers based on SOS diodes", *Pulsed Power Conference*, 992–998 (1997).

[32] V.A. Kozlov, I.A. Smirnova, S.A. Moryakova, and A.F. Kardo-Sysoev, "New generation of drift step recovery diodes (DSRD) for subnanosecond switching and high repetition rate operation", *Conference Record of the Twenty-Fifth International Power Modulator Symposium*, 441–444 (2002).

[33] M.S. Nikoo, S.M. Hashemi, and F. Farzaneh, "A Two-Stage DSRDBased High-Power Nanosecond Pulse Generator", *IEEE Transactions on Plasma Science* 46(2), 427–433 (2018).

[34] A.S. Kesar, "A Compact, 10-kV, 2-ns Risetime Pulsed-Power Circuit Based on Off-the-Shelf Components", *IEEE Transactions on Plasma Science* 46(3), 594–597 (2018).

[35] R. Fullwood, "On the Use of 2N504 Transistors in the Avalanche Mode for Nuclear Instrumentation", *Review of Scientific Instruments* 31(11), 1186–1189 (1960).

[36] M. Inokuchi, M. Akiyama, T. Sakugawa, H. Akiyama, and T. Ueno, "Development of Miniature Marx Generator using BJT", *IEEE Pulsed Power Conference (PPC)*, 57–60 (2009).

[37] T. Ohkami, M. Souda, T. Saito, C. Yamazaki, S.Asano, Y. Suzuki, A. Hayakawa, M. Osakabe, K. Nagaoka, Y. Takeiri, and O. Kaneko, "Development of a 40 kV Series-connected IGBT Switch", *Power Conversion Conference – Nagoya*, 1175–1180 (2007).

[38] Y. Achour, J. Starzyński, and A. Łasica, "New embedded nanosecond pulse generator based on spark gap and IGBT", *IEEE 21st International Conference on Pulsed Power (PPC)*, (2017).

[39] J.C. Pouncey, and J.M. Lehr, "A spark gap model for LTspice and similar circuit simulation software", *2015 IEEE Pulsed Power Conference (PPC)*, 1–6 (2015).

[40] R.J. Baker, "High voltage pulse generation using current mode second breakdown in a bipolar junction transistor", *Review of Scientific Instruments* 62(4), 1031–1036 (1991).

[41] S.J.V. Bright, S. Ramkumar, H. Anand, "Positive output elementary Luo converter for fixed-frequency ZVS operation", *Bull. Pol. Ac.: Tech*. 65(2), 255–262 (2017).

[42] Ferroxcube, 3F3 material specifications, ferrite 3F3 Datasheet, (2008).

[43] ANSYS, Inc. ANSYS Electronics Desktop, http://www.ansys.com/fr-fr/products/electronics/ansyselectronics- desktop.

[44] C. Basso, "Spice model simulates spark-gap arrestor", *EDN Magazine 1977*, 3–5 (1997).